II INTERNATIONAL CONFERENCE ON COMPUTATIONAL BIOENGINEERING
H. Rodrigues *et al.* (Eds.)
Lisbon, Portugal, September 14–16, 2005

SENSITIVITY OF BLOOD FLOW IN STENOSED CAROTID BIFURCATION

I. Larrabide*, P.J. Blanco*, S.A. Urquiza and R.A. Feijóo***

* Laboratório Nacional de Computação CientíficaLNCC/MCT, Av. Getúlio Vargas 333,
25651-075 Petrópolis - RJ, Brasil
e-mail: nacho@lncc.br, pjblanco@lncc.br, feij@lncc.br

** Laboratorio de Bioingeniería, Universidad Nacional de Mar del PlataAv. J.B. Justo 4302,
7600 Mar del Plata, Argentina
e-mail: santiagourquiza@fi.mdp.edu.ar

Keywords: Hemodynamics, Sensitivity, Stenosed carotid, Coupling 3D-1D.

Abstract. *It is well known that hemodynamic factors are strongly influenced by the arterial geometry. Combining computational fluid dynamics with three-dimensional medical data can be of valuable aid for studying blood flow characteristics in real geometries. In this manner it is possible to analyze the sensitivity of hemodynamic factors related to shape changes in vascular districts. In this work the quantification of these sensitivities for a carotid bifurcation with different degrees of stenosis was investigated. To this end a multidimensional 3D - 1D FEM model of the whole arterial tree is implemented. It comprises a 3D compliant model of the carotid bifurcation coupled with a 1D model for the remaining part of the arterial tree, which makes use of Windkessel models to implement boundary conditions at the arteries ends. With this approach, difficulties arising from the treatment of boundary conditions for the 3D model are naturally handled.*

As mentioned above, several carotid bifurcation geometries were analyzed. Three of them are based on a standard geometry and correspond to different degree of stenosis at the carotid sinus. A fourth model was obtained from a patient-specific angiography using different image segmentation and reconstruction techniques. Detailed flow patterns and other associated hemodynamic factors are provided for all these models. Finally, these data results are analyzed in order to determine how geometrical changes influence the hemodynamic conditions for each case studied.

1 INTRODUCTION

An increasingly number of research efforts has been tackling the problems associated to vascular diseases with the aim of improving therapeutic, prevention and diagnostic techniques. In this context, atherosclerosis is one of the most prevalent pathologies. Clinical investigations reveal that atheroma plaques are mainly localized in vascular districts where altered hemodynamic conditions are present [1, 2, 3]. These zones are characterized by irregularities in the blood flow structure, such as flow separation and reversal, as well as low oscillatory wall shear stresses. Due to *in vivo* experiments are limited by lots of practical and ethical obstacles, computational models play a decisive role in the progress of this research field.

Nowadays, it is possible to implement complex realistic computational models so as to provide a better understanding of the hemodynamic phenomena present in the human arterial system, at very low cost and without inconveniencing people. Arterial system modelling implies some challenging issues such as geometry reconstruction from medical images (MRI, CT, etc.)[1, 4, 5, 6, 7] and numerical solution of non-linear problems which involve the fluid-structure interaction between blood flow and compliant arterial walls. As local multidimensional models introduce artificial boundaries within the arterial tree[8, 9, 10], it is necessary to supply these models with proper boundary conditions, taking into account the interactions with the rest of the arterial system in a time dependant context. Thus, it is possible to use local representations so as to study the phenomena associated to the flow dynamics in districts such as bifurcations and other singularities. In this way, rather detailed descriptions of vortex development and wall shear stresses -among other relevant hemodynamic phenomena- may be obtained in those locations. In order to do this, appropriate coupling between complex 3D models and reduced 1D models must be considered. These 1D models are used to represent the rest of the arterial system supplying the 3D model with proper boundary conditions that take into account the systemic interactions. With this approach, boundary conditions for localized models will be naturally adjusted when changes occurs in any of the two models. This in turn, facilitates the implementation of different situations of practical interest with easy.

In this work, we used this approach to analyze flow conditions in the carotid bifurcation for different degrees of stenosis. Also, the standard geometry in normal conditions was compared with a real geometry so as to determine how local geometry influences hemodynamic factors.

2 GOVERNING EQUATIONS

In this section we present the governing equations for the 1D model, the 3D model and the 1D-3D coupling scheme.

2.1 THE 1D MODEL

By assuming appropriate simplification hypothesis on the geometry and flow characteristics in the blood flow through arteries, it is possible to obtain a one dimensional set of equations governing the blood flow in major arteries considering no flux across the wall. The result of this simplification is the following system of non-linear partial differential equations:

The 1D Model

Unidimensional flow in major vessels - System of equations

$$
\begin{aligned}
S_{,t} + (Sv)_{,x} &= 0 \\
(Sv)_{,t} + [v^2 S(1+\bar{\delta})]_{,x} + \tfrac{S}{\rho} p_{,x} &= vN + \tfrac{\mu}{\rho}(Sv)_{,xx} \\
p = p_0 + \tfrac{E\pi R_0 h_0}{S}\left(\sqrt{\tfrac{S}{S_0}} - 1\right) + \tfrac{k\pi R_0 h_0}{S}\tfrac{1}{2\sqrt{S_0 S}} S_{,t} \quad (1) \\
\textit{being } N = \tfrac{\mu}{\rho} \oint_{C(x,t)} \phi_{,m} dl \\
\textit{and } \bar{\delta} = \tfrac{1}{S}\int_S \phi^2 \, dA - 1
\end{aligned}
$$

were S represents the luminal area of the vessel, v the mean velocity of the blood and p is the mean pressure at a point x. We also denoted by ϕ the velocity profile across the transversal section S, $C(x,t)$ is the curve limiting S and m is the outward normal of $C(x,t)$.

An equation representing the wall response, considering a linear viscoelastic relation is used to close the system. In the equation for p, R_0 is the arterial radius, h_0 is the wall thickness and S_0 is the area. The three values R_0, h_0 and S_0 are referred to the reference pressure value p_0. E is the effective Young Modulus and k is the fluidity coefficient due to the parietal viscosity.

2.2 3D MODEL AND COUPLING EQUATIONS

Let Ω be the 3D region under consideration, $\mathbf{x} = (x_1, x_2, x_3)$ is a arbitrary point in Ω, $\mathbf{v} = \mathbf{v}(\mathbf{x}, t)$ represents the velocity of the blood flow, and $\mathbf{u}(\mathbf{x}, t)$ is the movement of the reference frame consistent with the ALE formulation. Then, from the Virtual Power Principle we have:

$$
\begin{aligned}
&\int_\Omega \rho \mathbf{v}_{,t} \cdot \hat{\mathbf{v}} \, d\Omega + \int_\Omega \rho \nabla \mathbf{v}(\mathbf{v} - \mathbf{u}) \cdot \hat{\mathbf{v}} d\Omega - \int_\Omega p \; div(\hat{\mathbf{v}}) \; d\Omega + \int_\Omega \mu \nabla \mathbf{v} \cdot \nabla \hat{\mathbf{v}} \; d\Omega = \\
= &\int_\Omega \mathbf{b} \cdot \hat{\mathbf{v}} - \sum_{i=1}^{n} \int_{S_i} p_{1D} \mathbf{n} \cdot \hat{\mathbf{v}} \; dS \quad \forall \hat{\mathbf{v}} \in Var_v \qquad (2) \\
&\int_\Omega div(\mathbf{v}) \hat{p} \; d\Omega = 0 \quad \forall \hat{p} \in Var_p \qquad (3)
\end{aligned}
$$

Being p_{1D} the tension on the coupling surface S_i from the 1D model. Then the variational problem can be posed as:

Variational Problem - 3D Incompressible Newtonian Fluid Flow

Given $\mathbf{b}$, find $\mathbf{v} \in Kin_v$ and $p \in Kin_p$ such that:

$$\begin{cases} (\mathbf{v}_{,t}, \hat{\mathbf{v}}) + a(\mathbf{v}, \hat{\mathbf{v}}) + \ b(\mathbf{v}, \mathbf{u}, \hat{\mathbf{v}}) \ + \ g(\hat{\mathbf{v}}, p) \ = \ (\mathbf{b}, \hat{\mathbf{v}}) \ + \ \sum_{i=1}^{n} \ c(\bar{p}_i, \hat{\mathbf{v}}) \\ g(\mathbf{v}, \hat{p}) = 0 \end{cases} \tag{4}$$

For Kin_v, Kin_p, Var_v e Var_p defined as:

$$\begin{aligned} Kin_v \ &= \{\mathbf{v} \in \mathcal{U} \ ; \ \mathbf{v} = 0 \ in \ \partial V_{\bar{\mathbf{v}}}\}, \quad Var_v \ = \{\hat{\mathbf{v}} \in \mathcal{V} \ ; \ \hat{\mathbf{v}} = 0 \ in \partial V_{\bar{\mathbf{v}}}\} \\ Kin_p \ &= \{p \in \mathcal{U} \ ; \ p = \bar{p}(t) \ in \ \partial V_{\bar{p}}\}, \quad Var_p \ = \{\hat{p} \in \mathcal{V} \ ; \ \hat{p} = 0 \ in \ \partial V_{\bar{p}}\} \end{aligned}$$

With initial condition $\mathbf{v}|_{t=0} = \mathbf{v}_0$, and:

$$\begin{aligned} a(\mathbf{v}, \hat{\mathbf{v}}) &= \mu(\nabla \mathbf{v}, \nabla \hat{\mathbf{v}}) \ a \ bilinear \ form \ in \ V; \\ b(\mathbf{v}, \mathbf{u}, \hat{\mathbf{v}}) &= ((\nabla \mathbf{v})(\mathbf{v} - \mathbf{u}), \hat{\mathbf{v}}) \ a \ trilinear \ form \ in \ V; \\ c(\bar{p}_i, \hat{\mathbf{v}}) &= -\textstyle\int_{S_i} p_{1D} \mathbf{n} \cdot \hat{\mathbf{v}} \ dS \ a \ bilinear \ form \ in \ V; \\ g(\hat{\mathbf{v}}, \hat{p}) &= -(div(\hat{\mathbf{v}}), \hat{p}); \\ \bar{p}_i &= mean \ pressure \ in \ the \ transversal \ section \ of \ \partial V_{\bar{p}}; \\ (\cdot, \cdot) &= usual \ internal \ product \ in \ \mathcal{U}. \end{aligned} \tag{5}$$

In order to complete this set of equations we need to provide proper boundary conditions and constitutive relations linking the pressure and the arterial wall displacement. In this case, a simple independent ring wall model consistent with that of the 1D model was chosen. Then, the following equations for the points over the surface $\partial\Omega$ (representing the arterial wall) were used:

$$\begin{aligned} p &= p_0 + \frac{Eh}{R_0^2}\gamma + \frac{kh}{R_0^2}\gamma_{,t} \\ \triangle \mathbf{x} &= \gamma \mathbf{n} \qquad\qquad in \ \partial\Omega \\ \mathbf{v} &= \mathbf{x}_{,t} \end{aligned} \tag{6}$$

where γ represents the displacements of the arterial wall in the direction $\mathbf{n}$ (the outward normal of the wall).

In order to couple the 1D and 3D model we have to introduce another set of equations on the interfaces between both models, which states for the proper coupling conditions regarding a well-posed problem as mentioned in [11]. In order to satisfy continuity of

mass we impose the following:

$$\mathcal{Q}_i \;=\; -\int_{S_i} \mathbf{v}\cdot\mathbf{n}\; dS \tag{7}$$

being $\mathcal{Q}_i$ the corresponding 1D flow rate at the coupling interface S_i. To satisfy the continuity of tensions in the 1D-3D interface we have:

$$\int_{\partial\Omega_i} T_{3D}\mathbf{n}\cdot\hat{\mathbf{v}}\; d\partial\Omega \;+\int_{S_i} p_{1D}\mathbf{n}\cdot\hat{\mathbf{v}}\; dS \;=\; 0,\; i=1,n \quad \forall\hat{\mathbf{v}}\in Var_v \tag{8}$$

where p_{1D} is the mean pressure given by the 1D model in the coupling interface S_i, T_{3D} is the stress tensor given by the 3D model in the coupling interface $\partial\Omega_i$ and $\mathbf{n}$ is the outward normal of $\partial\Omega_i$. These two equations imply continuity in mass and stress in the 1D-3D interface.

It is easy to show that, for high Reynold numbers, equation 8 implies continuity on pressure.

3 MODELS

3.1 One Dimensional Tree

The full arterial system was built using 128 segments (see Figure 1(a)). Geometrical and mechanical parameters are based on those proposed by Avolio in [12]. Regarding the parietal viscosity, it is defined the angle ϕ as $\phi = arctg\left(\frac{\omega k}{E}\right)$ where $\omega = \frac{2\pi}{T}$, being T the heart beat period. This parameter is a measure of the relative magnitude of the parietal viscosity force to the elastic one. For the inflow boundary condition, the flow ejected by the left ventricle at the aortic root was considered. In Figure 1(b) the curve used in this work is shown, taken from Stettler[13]. On bifurcations, continuity on pressure and flow is considered [14]. In order to include the action of the peripheral beds, lumped Windkessel models[14, 15, 16] are used. These elements comprise a resistance R_1 in series with the parallel of a resistance R_2 and a capacitor C. The values of the resistances are such that the flow distribution towards the different parts of the body is according to that given in [17], always verifying the relation $R_1 = 0.2R_T$[15, 16] with $R_T = R_1 + R_2$. The total peripheral compliance is taken from Stergiopulos[15]. This compliance is distributed on each Windkessel terminal following the same guidelines proposed there. The equation which corresponds to each terminal is as follows:

$$Q_{,t} = \frac{1}{R_1 R_2 C}\left[R_2 C p_{,t} + p - (R_1+R_2)Q\right] \tag{9}$$

The one-dimensional model has 1212 nodes and 1326 linear elements. Equations in system (1) are discretized by means of the Finite Element Method, using a Galerkin-Least Squares formulation over the characteristic lines corresponding to the normal equations associated with the resulting hyperbolic system when $k = 0$. Such scheme is operated

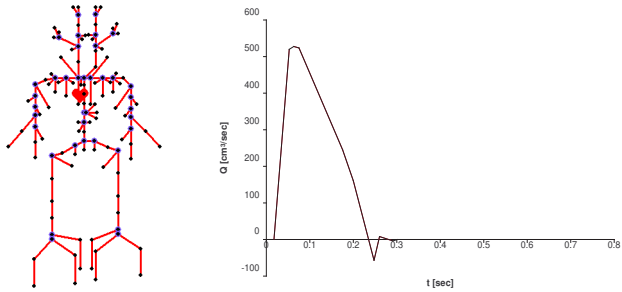

(a) 1D Tree topology (b) Heart outflow curve

Figure 1: One dimensional tree.

with a stabilization parameter corresponding to the optimal value for the SUPG[18] method. The implementation is made within the context of a framework[19] for the solution of discrete problems, which allows a simple and direct use of different kinds of elements despite their formulations or dimensions.

3.2 3D Model - Method

The Finite Elements Method is used to solve the above mentioned systems of equations for 3D domains. The domain is composed of P1b-P1 tetrahedral elements with bubble shape functions for the velocity field and linear shape functions for the scalar pressure field [20]. The solution is stabilized using the SUPG method. Temporal derivatives are solved with a θ-Euler implicit finite difference scheme, using Picard interations in order to treat the non-linear convective terms. The solution of the problem is split into three sub-steps: in the first one, the bubble degrees of freedom are eliminated by direct substitution and the 3D model problem is solved using the pressure values obtained in 1D model in the previous time step as boundary conditions. In the second sub-step, the solution for the 1D model is calculated with the flow rate values obtained from the multidimensional model in the first sub-step, and finally in the third step, we solve the bubble degrees of freedom to be used in the following time step. This coupling alternative does not require the calculation of the Riemann invariants in contrast with that proposed in [10]. The domain is updated from the position of the nodes on the surface -that are obtained from eq. (6)- solving a Laplace problem for each nodal coordinate.

3.3 3D Model - Standard Geometry

The 3D standard geometry (NCG) upon which three of the four cases presented in this work are based, was proposed by Bharadvaj et. al. [21]. This geometry was scaled to be consistent with the common carotid diameter value of the 1D model. From this geometry, two different classes of stenosis were considered as shown in Figures 2(a) and

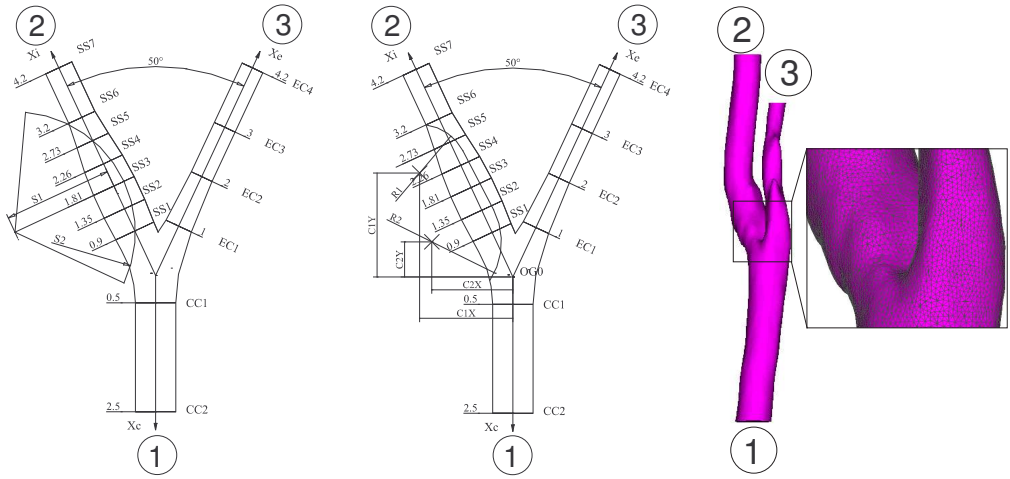

(a) Stenosis geometry A (SCGI) (b) Stenosis geometry B (SCGII) (c) Real carotid geometry (RCG)

Figure 2: Different geometries used.

2(b). These cases were named SCGI and SCGII respectively. In Table 1 the dimensions of both stenosis types are specified, and are such that the carotid sinus is 80%-stenosed regarding the reduction of the section SS3. The finite element meshes have 57009 nodes and 323711 elements for case NCG, 40373 nodes and 198154 elements for case SCGI and 38433 nodes and 208196 elements for case SCGII.

3.4 3D Model - Reconstructed Geometry

The real carotid geometry (case RCG) was acquired from a MRA. The input image was segmented using a novel segmentation method based on Topological Derivative [22]. From this segmentation, by means of Marching Cubes algorithm, the 3D mesh of the carotid artery internal wall was reconstructed. This initial mesh was post-processed to obtain the final surface mesh and then, using a frontal method, a tetrahedral mesh was constructed from the triangularized surface. The resulting mesh (94732 nodes, 638128 elements) is presented in Figure 2(c).

4 RESULTS

In this section computational results of this work are presented. Subsection 4.1 corresponds to the comparison between flow rate and pressure curves corresponding to a standard healthy carotid geometry and the two different stenosis mentioned above (Table 1).

Section	**SS1**	**SS2**	**SS3**	**SS4**	**SS5**	**SS6**	**SS7**
Diameter[cm]	0.77182	0.8214	0.8214	0.76368	0.6364	0.5254	0.5254
Section	**CC1**	**CC2**	**EC1**	**EC2**	**EC3**	**EC4**	
Diameter[cm]	0.74	0.74	0.51356	0.42032	0.42032	0.42032	
SCGI	**S1**	**S2**					
S[cm]	2	2.20535					
SCGII	**R1**	**R2**	**CX1**	**CY1**	**CX2**	**CY2**	
R/CX/CY[cm]	1.00555	3.11198	-1.711571	1.785855	-3.35534	0.375378	

Table 1: Dimensions corresponding to both stenosis geometries.

In subsection 4.2 the same curves, for the standard healthy geometry and the real carotid (shown in Figure 2(c)), are compared. In order to correlate results to the feasibility of development of stenosis with flow patterns, the oscillating shear stresses index (OSI[23]) was calculated as follows:

$$OSI \;=\; \frac{1}{2}\left[1 - \frac{\left|\int_0^T \tau dt\right|}{\int_0^T |\tau| dt}\right] \tag{10}$$

where T is the cardiac period, and τ is the wall shear stress tensor.

4.1 Different Stenosis Geometries

As mentioned, the standard carotid geometry (NCG) and the two different stenosis geometries SCGI and SCGII (Figure 2), are compared. For each case the pressure and flow rate curves were compared at the Common Carotid Artery (CCA, labelled as ①) and after the carotid bifurcation, at the Internal Carotid Artery (ICA, labelled as ②) and External Carotid Artery (ECA, labelled as ③). It can be seen from these curves that the arterial pulse and flow rate does not suffer significant perturbations.

4.2 Real Geometry vs. Standard Geometry

In this section we compare the NCG with the RCG. For each case the pressure and flow rate curve were compared at the same points mentioned above. No major differences were found in the shape of the curve besides that, for the real carotid, the flow rate and pressure maximum (and minimum) does not reach the same value as in the case of the standard geometry.

Finally, the distribution of the OSI for the different geometries is presented in Figure 4.2. Strong variations of blood flow direction are associated to values of the OSI close to 0.5.

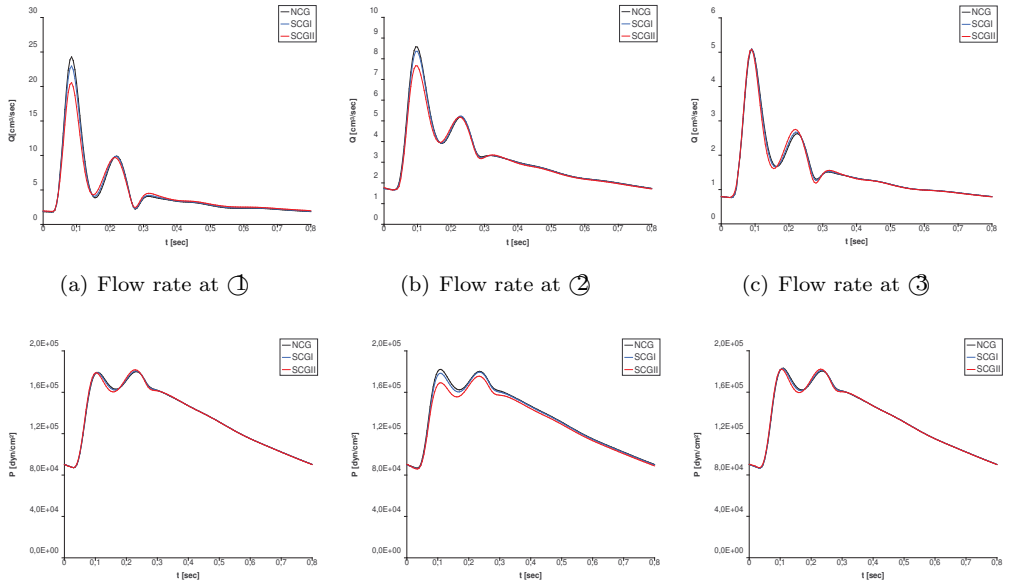

(a) Flow rate at ①

(b) Flow rate at ②

(c) Flow rate at ③

(d) Pressure at ①

(e) Pressure at ②

(f) Pressure at ③

Figure 3: Flow rate and Pressure at CCA ① , ICA ② and ECA ③ for the standard geometry with different stenosis(NCG, SCGI and SCGI).

5 CONCLUSIONS

In this work, by means of a coupled 1D-3D model, a comparison between different degrees of stenosis at the carotid bifurcation using an standard geometry and a geometry obtained form a patient-specific MRA was performed. The aim of this comparison was to quantify the sensitivity of hemodynamic factors such as flow rate, pressure and OSI.

As shown by Figures 4.1 and 4.2 the flow rate and pressure curves are not substantially affected by changes in the geometry.

On the other hand, the flow pattern is strongly dependent of the geometry as evidenced by the comparison of the OSI shown in Figure 4.2.

ACKNOWLEDGEMENTS

This research was partly supported by FINEP/CNPq-PRONEX Project under Contract 664007/1997-0, by MCT/PCI-LNCC Project. Pablo Javier Blanco and Ignacio Larrabide were partly supported by the brazilian agency CNPq. The support from these agencies is greatly appreciated.

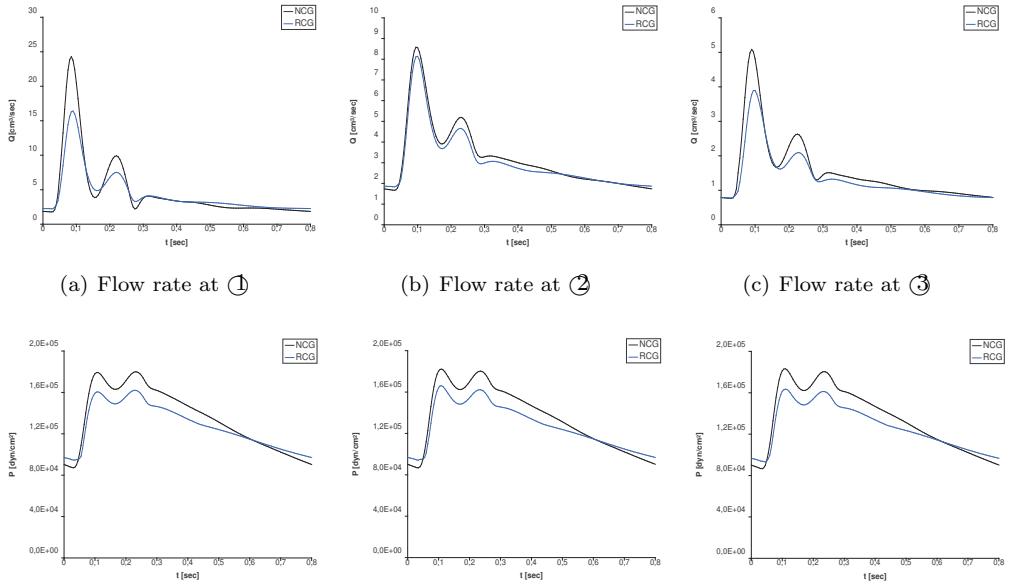

(a) Flow rate at ①

(b) Flow rate at ②

(c) Flow rate at ③

(d) Pressure at ①

(e) Pressure at ②

(f) Pressure at ③

Figure 4: Flow rate and Pressure at CCA ① , ICA ② and ECA ③ for the standard and real geometry(NCG and RCG).

REFERENCES

[1] C.G. Caro, J.M. Fitz-Gerald, R.C. Schroter, "Atheroma and arterial wall shear dependent mass transfer mechanism for atherogenesis", Proc. Royal Society of London, Biology, 1971, 177:109-159.

[2] S. Hyun, C. Kleinttreuer, J.P. Jr. Archie, "Hemodynamics analyses of arterial expansions with implications to thrombosis and restenosis", Medical Engineering & Physics, 2000, 22:13-27.

[3] D.N. Ku, D.P. Giddens, C.K. Zarins, S. Glagov, "Pulsatile flow and atherosclerosis in the human carotid bifurcation. Positive correlation between plaque location and low oscillating shear stress", Ateriosclerosis, 1985, 5:293-302.

[4] M.J. Vénere, R.A. Feijóo, "Generación de Mallas a Partir de Tomografías", MECOM99, Mendoza, Argentina,1999.

[5] J.R. Cebral, P.J. Yim, R. Löhner, O. Soto, P.L.Choyke, "Blood Flow Modeling in Carotid Arteries with Computational Fluid Dynamics and MR Imaging", Academic Radiology, 2002, 9-11:1286-1299.

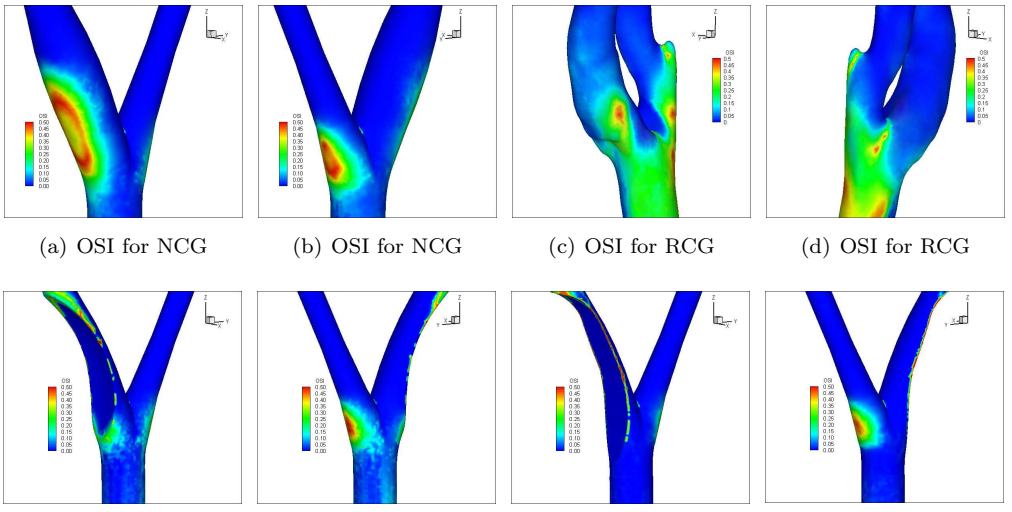

(a) OSI for NCG (b) OSI for NCG (c) OSI for RCG (d) OSI for RCG

(e) OSI for SCGI (f) OSI for SCGI (g) OSI for SCGII (h) OSI for SCGII

Figure 5: OSI for the real and standard geometry.

[6] F. Calamante, P.J. Yim, J.R. Cebral, "Estimation of bolus dispersion effects in perfusion MRI using image-based computational fluid dynamics", NeuroImage, 2003, 19:341-353.

[7] R. Botnar, G. Rappitsch, M.B. Scheidegger, D. Liepsch, K. Perktold, P. Boesiger "Hemodynamics in the carotid artery bifurcation: a comparison between numerical simulations and in vitro MRI measurements", J. of Biomech., 2000, 33:137-144.

[8] A. Quarteroni, "Modeling the cardiovascular system: a mathematical challenge", Mathematics Unlimited - 2001 and Beyond, B. Engquist and W. Schmid Eds, Springer-Verlag, 2001, 961-972.

[9] L. Formaggia, J.F. Gerbeau, F. Nobile, A. Quarteroni, "On the coupling of 3D and 1D Navier-Stokes equations for flow problems in compliant vessels", Comp. Meth.App. Mech & Eng., 2001, 191:561-582.

[10] L. Formaggia, F. Nobile, J.F. Gerbeau, A. Quarteroni, "Numerical treatment of defective boundary conditions for the NavierStokes equations" , EPFL-DMA Analyse et Analyse Numerique Report, 2000, 20.

[11] S. Urquiza , P. Blanco , G. Lombera, M. Venere and R. Feijo. "Coupling Multidimensional Compliant Models For Carotid Artery Blood Flow". Mecnica Computacional Vol. XXII, M. B. Rosales, V. H. Cortnez y D. V. Bambill (Editores)-AMCA, Baha Blanca, Argentina, 2003, 232-243.

[12] A.P. Avolio, "Multi-branched model of the human arterial system", Med. Biol. Eng. Comp., 1980, 18:709-718.

[13] J.C. Stettler, P. Niederer, M. Anliker, "Theoretical analysis of arterial hemodynamics including the influence of bifurcations", Annals of Biomedical Engineering, 1980.

[14] M.S. Olufsen, "Structured tree outflow condition for blood flow in large systemic arteries", Am. J. Physiol., 1999, 276:257-268.

[15] N. Stergiopulos, D.F. Young, T.R. Rogge, "Computer simulation of arterial flow whit applications to arterial and aortic stenoses", J. of Biomechanics, 1992, 25:1477-1488.

[16] F. Otto, "Die Grundform des arteriellen pulses". Zeitschrift für Biologie, 1899, 37:483-529.

[17] W.W. Nichols, M.F. ORourke, "McDonalds Blood Flow in Arteries: Theoretical, Experimental and Clinical Principles" Forth Edition, Arnold and Oxford Univ. Press, 1998.

[18] T.J.R. Hughes, A. Brooks, "A theoretical framework for Petrov-Galerkin methods with discontinuos functions: Application to the stream-upwind procedure", Finite Element in Fluids IV, Wiley, London, 1982, 46-65.

[19] S.A. Urquiza, M.J. Venere, "An application framework architecture for FEM and other related solvers", MECANICA COMPUTACIONAL , S. Idelsohn, V. Sonzogni, A. Cardona Eds., CERIDE, Sta. Fe, Argentina, 2002, 21:3099-3109.

[20] O. Pironneau, "Finite-element methods for fluids", Wiley, New York, 1989.

[21] B.K. Bharadvaj, R.F. Mabon, D.P. Giddens, "Steady flow in a model of the human carotid bifurcation-I. Flow Visualization", J. of Biomechanics, 1982, 15:349-362.

[22] I. Larrabide, R.A. Feijóo, A.A. Novotny, E. Taroco, M. Masmoudi, "An image segmentation method based on a discrete version of the Topological Derivative", Proc. World Congress Structural and Multidisciplinary Optimization 6, ISSMO, Rio de Janeiro, 2005.

[23] D.N. Ku, D.P. Giddens, C.K. Zarins, S. Glagov, "Pulsatile flow and atherosclerosis in the human carotid bifurcation. Positive correlation between plaque location and low oscillating shear stress", Ateriosclerosis, 1985, 5: 293-302.